The contribution of coccolithophores to the optical and inorganic carbon budgets during the Southern Ocean Gas Exchange Experiment: New evidence in support of the "Great Calcite Belt" hypothesis

W. M. Balch,[1] D. T. Drapeau,[1] B. C. Bowler,[1] E. Lyczskowski,[2] E. S. Booth,[1] and D. Alley[1]

Received 4 January 2011; revised 14 April 2011; accepted 21 April 2011; published 4 August 2011.

[1] We describe optical observations from the Southern Ocean (SO) Gas Exchange Experiment (GasEx) during March 2008, designed to test the hypothesis that enhanced reflectance of the Southern Ocean waters was related to a high abundance of coccolithophorids. We present multiple lines of evidence in support of this hypothesis: (1) birefringence microscopy, (2) along-track measurements of acid labile backscattering, (3) analytical measurements of particulate inorganic carbon (PIC), and (4) above-water radiometry measurements made from both ship and satellite. At the SO GasEx study site (~51°S, 38.5°W) coccolithophores and coccoliths were abundant (~300 cells mL^{-1} and 20,000 coccoliths mL^{-1}) and concentrations were stable over time scales of weeks. Enhanced concentrations of PIC were observed between the Subtropical Front (STF) and the northern part of the Subantarctic Front (SAF) and between the SAF region and Polar Front. Biogenic silica was elevated with the highest concentrations south of the STF. These results, along with other recent microscope observations of coccolithophores made by other workers around the Southern Ocean, suggest that the region of enhanced reflectance is, at least partially, due to coccolithophores. However, the PIC estimated from above-water reflectance measurements was 2–3X the PIC actually measured in the water. One possible reason for this is the presence of other sources of scattering, such as microbubbles (at least during stormy conditions). These observations are consistent with the hypothesis that this region of elevated reflectance and PIC is part of a significantly larger region which encircles the entire Southern Ocean each austral summer, a band that we call the "Great Calcite Belt."

Citation: Balch, W. M., D. T. Drapeau, B. C. Bowler, E. Lyczskowski, E. S. Booth, and D. Alley (2011), The contribution of coccolithophores to the optical and inorganic carbon budgets during the Southern Ocean Gas Exchange Experiment: New evidence in support of the "Great Calcite Belt" hypothesis, *J. Geophys. Res.*, *116*, C00F06, doi:10.1029/2011JC006941.

1. Introduction

[2] Coccolithophores are calcium carbonate ($CaCO_3$)-producing phytoplankton (class Prymnesiophyceae) that significantly influence carbon chemistry and impact global biogeochemical cycles. There is a close correlation between sinking organic carbon and $CaCO_3$, suggesting that $CaCO_3$ acts as ballast for much of the export production of organic carbon to the deep sea [*Armstrong et al.*, 2001; *Francois et al.*, 2002; *Klaas and Archer*, 2002]. The balance of two common biogenic minerals in seawater, $CaCO_3$ and biogenic silica (from diatom frustules) appears to be a strong controller of the sinking rates of particulate matter [*Balch et al.*, 2010].

[3] Blooms of the cosmopolitan coccolithophore *Emiliania huxleyi* have been studied mostly in the Northern Hemisphere [*Balch et al.*, 1991; *Broerse et al.*, 2003; *Holligan et al.*, 1993, 1983b; *Iida et al.*, 2002; *Wal et al.*, 1995]. However, coccolithophore blooms are found globally in the higher-latitude waters of both hemispheres [*Brown and Yoder*, 1994]. Most of the blooms are from the species *Emiliania huxleyi*, but other coccolithophores also can cause them [*Tyrrell and Merico*, 2004]. Coccolithophores, while considered to belong to a single functional group (i.e., calcifying algae), inhabit a variety of hydrographic and light conditions [*Young*, 1994].

[4] Even within the ubiquitous species *E. huxleyi*, conditions selecting for coccolithophore blooms are unclear. Phosphate limitation has been hypothesized to be a critical factor promoting blooms [*Paasche and Brubak*, 1994; *Riegman et al.*, 1992, 2000; *Townsend et al.*, 1994], based

[1]Bigelow Laboratory for Ocean Sciences, West Boothbay Harbor, Maine, USA.
[2]School of Marine Sciences, University of Maine, Orono, Maine, USA.

0148-0227/11/2011JC006941

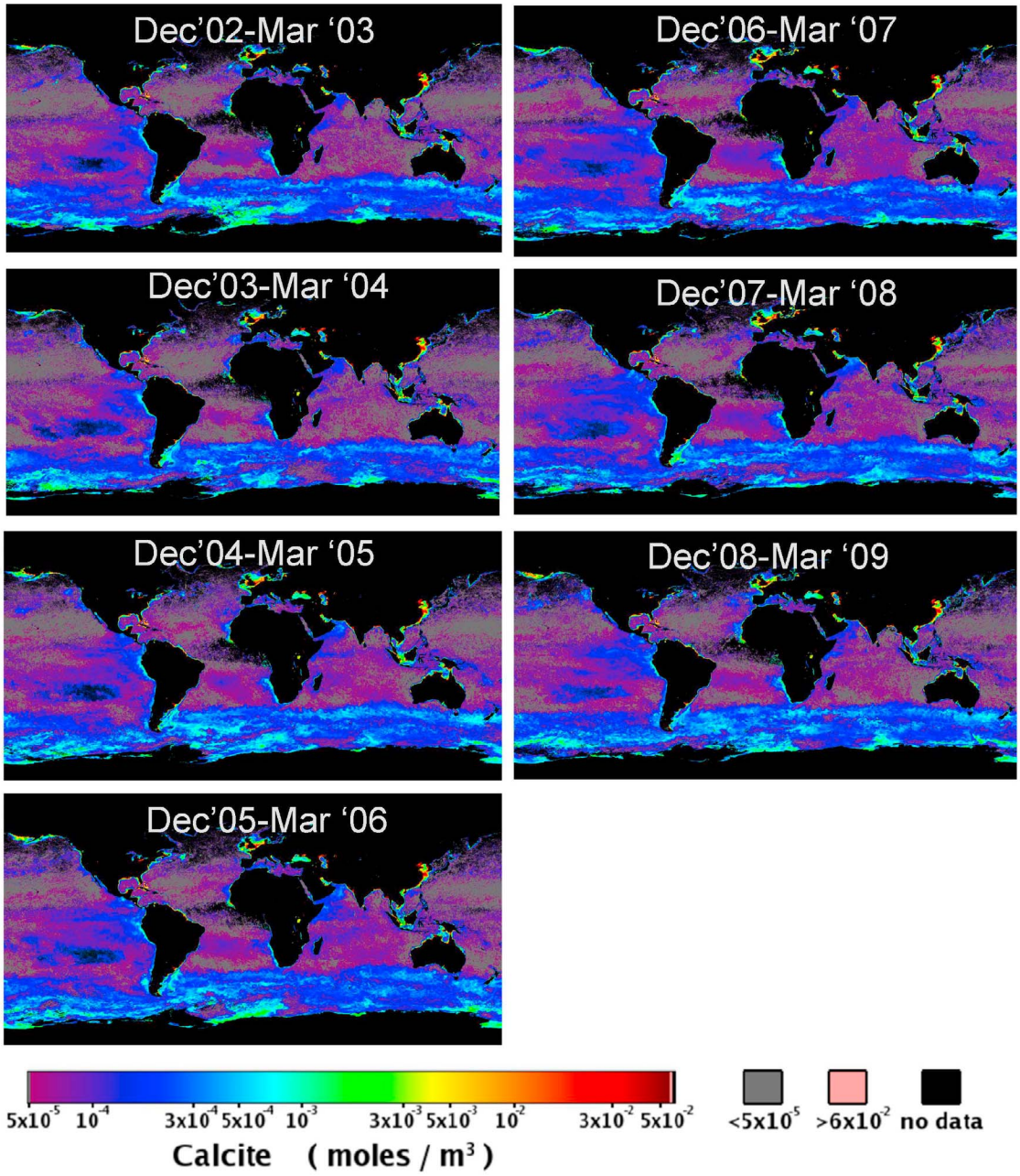

Figure 1. Moderate Resolution Imaging Spectroradiometer (MODIS)-Aqua images processed for particulate inorganic carbon (PIC) concentration (mol PIC m^{-3}) using the merged PIC algorithm [*Balch et al.*, 2005; *Gordon et al.*, 2001]. Color bar is shown at the bottom. Seasonal composite images for 21 December to 21 March (austral summer) are shown for 2003–2009. The Great Calcite Belt appears every year. Elevated values immediately adjoining the Antarctic continent are likely not PIC but of terrigenous origin (possibly glacial flour?). No shipboard data exist to validate this however.

on physiological studies indicating that *E. huxleyi* has an exceptionally high affinity for orthophosphate and may be able to utilize organic phosphorous using extracellular phosphatases [*Satoh et al.*, 2009; *Xu et al.*, 2006].

[5] Observations from Pacific blooms (eastern Bering Sea 1997–2000) led to a complete revision of the relationships between nutrient availability and coccolithophore bloom formation [*Merico et al.*, 2004; *Tyrrell and Taylor*, 1995] because the Bering Sea was found to be strongly nitrate limited [*Lessard et al.*, 2005], contrary to the above hypothesis on phosphate limitation [*Riegman et al.*, 2000; *Tyrrell and Taylor*, 1996]. Further, *E. huxleyi* blooms are favored in conditions with moderate stratification and occur within a few weeks of the summer solstice in each respective hemisphere [*Balch*, 2004].

[6] The advent of the particulate inorganic carbon (PIC) remote sensing algorithm for space-based measurements allowed, for the first time, quantitative estimates of cocco-

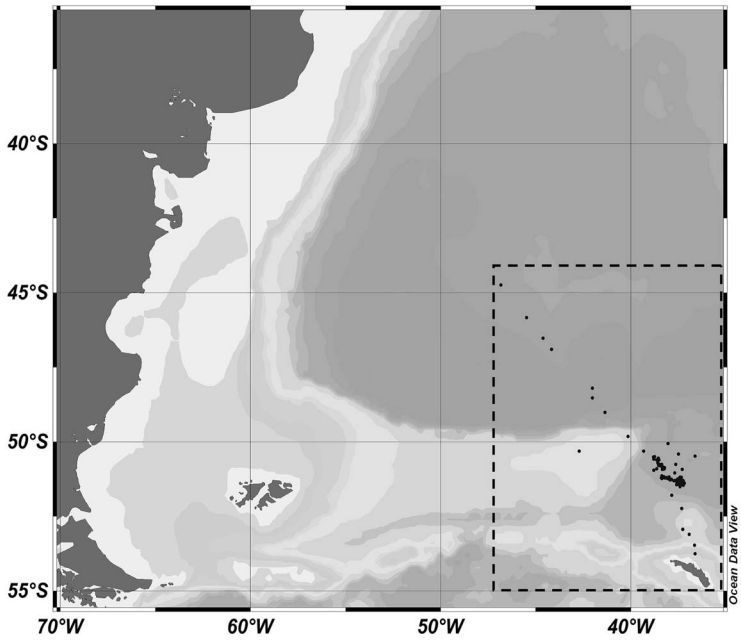

Figure 2. Study area for this work. Dots show positions of discrete analyses done along track. Background bathymetry is also shown (darker colors represent deeper water). Dashed box refers to same box shown in Figure 4.

lithophore PIC concentrations in bloom and nonbloom waters alike [*Balch et al.*, 2005; *Gordon et al.*, 2001] and global PIC time series have resulted. A consistent feature in all the global PIC imagery collected during the Moderate Resolution Imaging Spectroradiometer (MODIS)-Aqua mission has been what appears to be elevated PIC concentrations near the Subantarctic Front (SAF) and Polar Front (PF), all the way around the Southern Ocean. This large band of elevated PIC water, which we call the "Great Calcite Belt," has been observed for all years since the launch of MODIS-Aqua, with minor variation (Figure 1). The region of apparent elevated PIC appears south of the ~30°S parallel and extends southward to ~60°S with a total area of ~88×10^6 km^2. Satellite-derived PIC concentrations appear to be highest just east of the Drake Passage and gradually diminish with still measurable concentrations through the Indian and Pacific sectors of the Southern Ocean. Global models of *E.huxleyi* indeed predict increased abundance in the Great Calcite Belt [*Gregg and Casey*, 2007], in agreement with the coccolithophore flag algorithm for SeaWiFS [*Brown and Yoder*, 1994]. If this feature were really due to coccolithophorids, it could represent the largest water mass characterized by elevated abundance of Haptophyte algae in the world ocean.

[7] Another aspect revealed by the analysis of global PIC images is that coccolithophores are disproportionately more abundant in the Southern Hemisphere, particularly during austral summer. Indeed, 69% of the globally integrated PIC standing stock falls south of the equator from January to March and 43% of global suspended PIC is found poleward of 30°S, which represents 30% of the global ocean [*Balch et al.*, 2005].

[8] There is an alternative hypotheses for the higher than average reflectances in this region of the Southern Ocean. That is, that storm-induced microbubble injection [*Zhang et al.*, 2002], not PIC, is responsible for the high reflectance (see related paper by K. Randolph et al. (Optical measurements of bubble size distributions at 6–9 m depths generated by large-scale breaking waves in the Southern Ocean, submitted to *Journal of Geophysical Research*, 2011)).

[9] The work reported here was done as part of the Southern Ocean (SO) Gas Exchange Experiment (GasEx), which took place 29 February to 12 April 2008. The primary questions of the overall program were to determine, in Lagrangian-tracked patches, the gas transfer velocities at high winds as well as to measure the effect of biological, physical and chemical processes on gas exchange and pCO_2. Our measurements were focused on the optical properties of this patch and associated changes over time in particulate organic and inorganic particles. Our work was designed to examine the importance of calcium carbonate-producing coccolithophores to the overall optical properties of the region. Specifically, our goals were to (1) estimate the concentrations of coccoliths and PIC at the SO GasEx site in the Southern Ocean and examine the variability of their standing stocks over time, (2) examine the PIC contribution to the total particulate backscattering, (3) determine whether PIC coccoliths were present in sufficient quantities to elevate the reflectance in the Southern Ocean, (4) examine whether changes in the PIC standing stock in the mixed layer of the SO GasEx patches reflected alkalinity changes also observed over the same time period, and (5) examine the variability of another biogenic mineral, biogenic silica, and its relative variability throughout this region.

2. Methods

2.1. Overview of Sampling Strategy

[10] The cruise track of the R/V *Ron Brown* is shown in Figure 2. Two Lagrangian patches were followed, the first

was at 50.6°S, 38.6°W, initiated on 7 March 2008 and the second was at 51.1°S and 38.5°W, initiated on 21 March 2008. Both regions had a mixed layer of 60–70 m. Tracer for each patch (^{3}He and SF6) consisted of a 4000 L of surface ambient seawater, dispersed and subsequently measured as described by *Ho et al.* [2011]. Determination of the patch center was based on the position of the maximum SF6 tracer concentration as determined during regular steaming of a "pinwheel" survey through the patch area (Ho et al., submitted manuscript, 2011). The first patch experiment had to be terminated prematurely due to technical difficulties with the ship and an approaching storm and the ship headed to the lee of S. Georgia Island for several days. The ship then returned to the second experimental site to create and follow another patch.

2.2. Continuous Underway Measurements

[11] A continuous underway sampling system was utilized for this work which was connected to the ship's nontoxic sampling line, fed through a vortex debubbler. Sample variables included temperature and salinity (Sea-Bird conductivity and temperature sensor), chlorophyll *a* fluorescence (WET Labs WETStar fluorometer) and backscattering at 531 nm (WET Labs ECO-VSF sensor). Total particulate backscattering (b_{bp}) was measured by aiming the ECO-VSF into a sealed 2 L PVC chamber with angled end cap which helped reduce internal reflections). For the latter setup, to correct for any wall effect, 0.2 um filtered Milli-Q water was circulated through the system as a blank. Linearity of the optical measurements as a function of suspended particulate matter was confirmed through both a WETLabs ac-9 attenuation/absorption meter and the ECO-VSF using serial, sequential additions of Maalox© (a nonspectral scattering agent). These were used to verify the linearity of volume scattering at the three volume scattering sensors (100°, 125°, and 150°) as well as calculated particulate backscattering (b_{bp}) and beam attenuation at 9 wavelengths. Correlation coefficients (r^2) between beam attenuation and backscattering were never below 0.9997 for five point determinations between a range of particle beam attenuation of 0–4.27 m^{-1}. The ECO-VSF was factory calibrated prior to the cruise. The calculation of particle backscattering involved sampling the VSF at the three angles, subtracting the respective dark currents for each sensor as well as measurements of the MilliQ blank (to correct for the wall effect). No correction was made for the 30% enhancement of backscattering of seawater versus pure water [*Zhang et al.*, 2009]. This was because of the difficulties of generating optically pure, particle-free water and seawater on board ship. Experience has shown that the filtered Milli-Q water was likely elevated from the theoretical, pure water value (closer to the value of filtered pure seawater, regardless). Calibration constants converted the counts from each ECO-VSF sensor to volume scattering units (m^{-1} sr^{-1}). A fourth-order polynomial curve was fit to the three angles of volume scattering and integrated in order to estimate the total backscattering. It made no difference whether the wall effect was corrected by subtracting the blank for each angular sensor before integration or by subtracting the integrated blank value from the integrated measured backscattering.

[12] Acid-labile backscattering was measured with the ECO-VSF every 8–9 min using this system. The pH was lowered using a weak acid (10% glacial acetic acid) and PIC particles were dissolved as they traversed through a static mixer before the water entered the sensor volume. Once the pH downstream of the ECO-VSF sensor stabilized at <5.8, below the dissociation point for both aragonite and calcite, b_{bp} was remeasured. The difference between total and acidified b_{bp} represented "acid-labile backscattering" (b_b'). By using the same photometer for acidified and unacidified measurements, this eliminated issues associated with intercalibration of two scatterometers and caused only minor spatial aliasing in the b_b' measurement [*Balch et al.*, 2001]).

[13] The above-water radiance distribution was measured using a Satlantic MicroSAS system with seven wavelength radiance sensors (412, 443, 490, 510, 531, 555, 670 nm) for water and sky radiance measurements plus a spectral irradiance sensor (with cosine collectors, the same seven spectral bands) for measuring downwelling spectral irradiance. The radiance sensors viewed the water and sky at 40° from nadir and zenith, respectively. They also continuously viewed 120° from the solar azimuth (as per published protocols [*Mueller et al.*, 2003]) using an automated pointing system (based on positional and time information). Radiometric measurements of the seawater were taken far ahead of the bow wake and not subject to ship shadow. The instruments were factory calibrated before the cruise, and calibrations were tracked throughout the cruise using a 2% reflectance Spectralon plaque held horizontally below the water radiance sensor. Data were collected at 10 Hz over the cruise. White cap and bubble-contaminated data were eliminated by accepting only the lowest 5% of the radiometric data.

2.3. Discrete Analyses

[14] Discrete samples were taken from the CTD rosette for: particulate inorganic carbon (0.2 L seawater samples filtered onto 0.4 um pore size polycarbonate filters, rinsed with potassium tetraborate buffer [*Poulton et al.*, 2006]) and biogenic silica (0.5 L seawater sample filtered onto 45 mm 0.4 μm polycarbonate filters, stored and measured according to *Brzezinski and Nelson* [1989]), and coccolithophore/detached coccolith counts (using polarized light microscopy [*Haidar and Thierstein*, 2001]).

[15] The coccolith and coccolithophore technique involved first running 50 mL seawater onto a 0.45 um pore-size Millipore HA filter. Filters were immediately frozen at −20°C. Back on shore, samples were dried in a drying oven at 60°C for 24 h. Canada Balsam (0.2 mL) was placed on a glass microscope slide heated to 60°C on a warming plate. The sample filter was then carefully placed, facing upward, on the drop of heated Canada Balsam which was allowed to soak through the filter. Once evenly dispersed, a coverslip was carefully placed on top. Coccoliths viewed in a polarizing microscope (with two polarizers placed orthogonally, show up as bright particles against a dark field). Slides were automatically imaged using an Olympus BH2 microscope equipped with a 40X objective and 10X ocular (and camera "eye piece" attached to a QImaging-QuickCam Fast 1394 cooled monochrome, 12 bit digital camera. Image acquisition software controlled the stage and focus. For each image, the microscope software ran a "Z stack" of images through the optimal focal plane, then estimated the best focused image and saved that particular image. Two hundred images of each filter were taken for enumeration of plated cocco-

lithophores and detached coccoliths. Prior to coccolith enumeration, each image was viewed by a trained individual in order to verify focus and eliminate any poorly focused images.

[16] Enumeration of detached coccoliths and coccolithophorids was performed by software "CCC." The software first characterized the filter background pixel brightness based on the fraction of the image with pixel counts below a preset threshold, and estimated the standard deviation for multiple adjoining pixels below this specific level. Next, particles significantly above background but with diffuse boundaries and low levels of contrast (characteristic of detritus) were identified. Brightest pixels (aka "hills") with sharper gradients in birefringence light intensity then were identified, sized, distances to nearest hills determined as well as the angles between multiple hills within a given size range. These particles were classified based on the number of bright spots visible, as well as the angles between the individual points of light (detached coccoliths were subclassified as singlets (single points of light), doublets (double points within 0.3–3 μm distance), triple (three points, each 0.3–3 μm distance of each other) and quads (four birefringent spots, each 0.3–3 μm distance from each other). Plated cells and coccolith aggregates (PCCAs) were enumerated based on the frequency of birefringent spots within a radius of 6 μm. The intensity and area of each birefringent particle was also quantified.

[17] Accuracy and precision of the coccolith enumeration technique was verified by comparing machine counts of coccoliths, plated coccolithophores, and coccolith aggregates with manual counts from the same images. Statistics were evaluated using a simple power regression model, estimating the standard error associated with intercepts and slopes as well as the correlation coefficients. Significance levels of the statistical fits were evaluated using the F distribution and comparing to critical values of F [*Zar*, 1974]. For results reported here, all counts were related back to manual counts of imaged particles using the calculated regression coefficients.

3. Results

3.1. Coccolith Enumeration Method

[18] Machine counts of total birefringent particles as well as individual categories of the different categories of birefringent coccoliths (singlets, doublets, triplets, and quadruplets) plus PCCAs showed squared correlation coefficients (r^2) of 0.77–0.90 (based on a total of 138 image comparisons taken from 10 water samples between manual and machine counts; Figure 3). Machine counts of quadruplet and doublet birefringent particles plus PCCAs were generally higher than manual counts of the same images. Singlets and triplets, on the other hand, were closer to the 1:1 line (Figure 3). Data were fit with a power fit ($Y = AX^B$). A summary of the statistics of each regression and regression significance is given in Table 1, as well as in Figure 3. These relationships were used to convert automated microscope counts to manual count equivalents. CCC had difficulty discerning between aggregates of coccoliths and plated cells, and for this reason, those counts are combined, henceforth.

3.2. Satellite Imagery

[19] Broad scale MODIS-Aqua imagery showed that the SO GasEx study area was embedded within the broad scale circulation associated with the Subantarctic Frontal region [*Holligan et al.*, 2010] (see plus and cross symbols in Figure 4a which denote the first and second patch locations, respectively). Overall, it can be seen that there was a SW to NE temperature gradient through the study area. There were two frontal boundaries associated with the SAF region (here designated SAF_1 (at 12°C) and SAF_2 (at 6°C). The two patches were closest to SAF_2. Such a double frontal boundary near the SAF was also described by *Tsuchiya et al.* [1994] evident at SST of ~12°C and ~6°C (see their Figure 1). Further still to the north was the Subtropical front (STF) at 16°C. At the SE corner of our study area, the Polar Front (PF) was associated with 3°C water [*Holligan et al.*, 2010] and south of that, the Southern Antarctic Circumpolar Current Front (SACC) at ~1°C.

[20] The MODIS-Aqua chlorophyll data showed some coherence with the frontal boundaries as defined by SST, especially for the SAF_1, SAF_2, and the PF (Figure 4b) but not the STF. That is, chlorophyll levels north of SAF_1 and south of SAF_2 were greater than between SAF_1 and SAF_2. PIC concentrations, on the other hand, showed similar relative pattern to chlorophyll, but with stronger coherence with the SST-defined frontal features (Figure 4c). For example, PIC increased sharply south of the STF and north of SAF_1. Elevated PIC was also observed between SAF_2 and the PF.

3.3. Continuous Surface Underway Measurements

[21] The Subantarctic Front was clearly visible in the temperature and salinity data, with warm (>12°C; Figure 5a) salty (>34.5; Figure 5b) water to the north and colder fresher water to the south. The Polar Front (PF) was visible to the south in the temperature and salinity data, poleward of which showed the coldest water (<4°C), with salinities of ~34. Chlorophyll *a* fluorescence (calibrated to discrete chlorophyll; $\mu g\ L^{-1}$) north of the SAF were 2–5 $\mu g\ L^{-1}$. South of the PF, however, chlorophyll concentrations were <1–4 $\mu g\ L^{-1}$. In the region between the two fronts (the primary study site) the chlorophyll concentrations were patchy, ranging from 1 to 6 $\mu g\ L^{-1}$. Underway acid-labile backscattering (Figure 5d) showed peak values north of the SAF_1 as well as patchy, but significant, quantities in the region of the two Lagrangian patch experiments. Lowest b_b' values were observed during the transect to South Georgia Island (between patches 1 and 2), moderate values were observed in the study area and highest values were seen just to the north of the study site, at 48°S (Figure 5d). Total backscattering values were between 0.002 and 0.004 m^{-1} with highest values at the far northern part of the study area (Figure 5e). Chlorophyll concentrations based on the shipboard SAS, above-water radiometry using the OC-4 algorithm (Figure 5f), obviously were limited to only the daylight hours from roughly 1000–1400 LT, when the solar elevation was >20° above the horizon (hence there were fewer data overall than for other underway estimates of inherent optical properties such as backscattering). These results showed chlorophyll concentrations of 1–2 $\mu g\ L^{-1}$ in the study area and lowest values south of the PF. The PIC

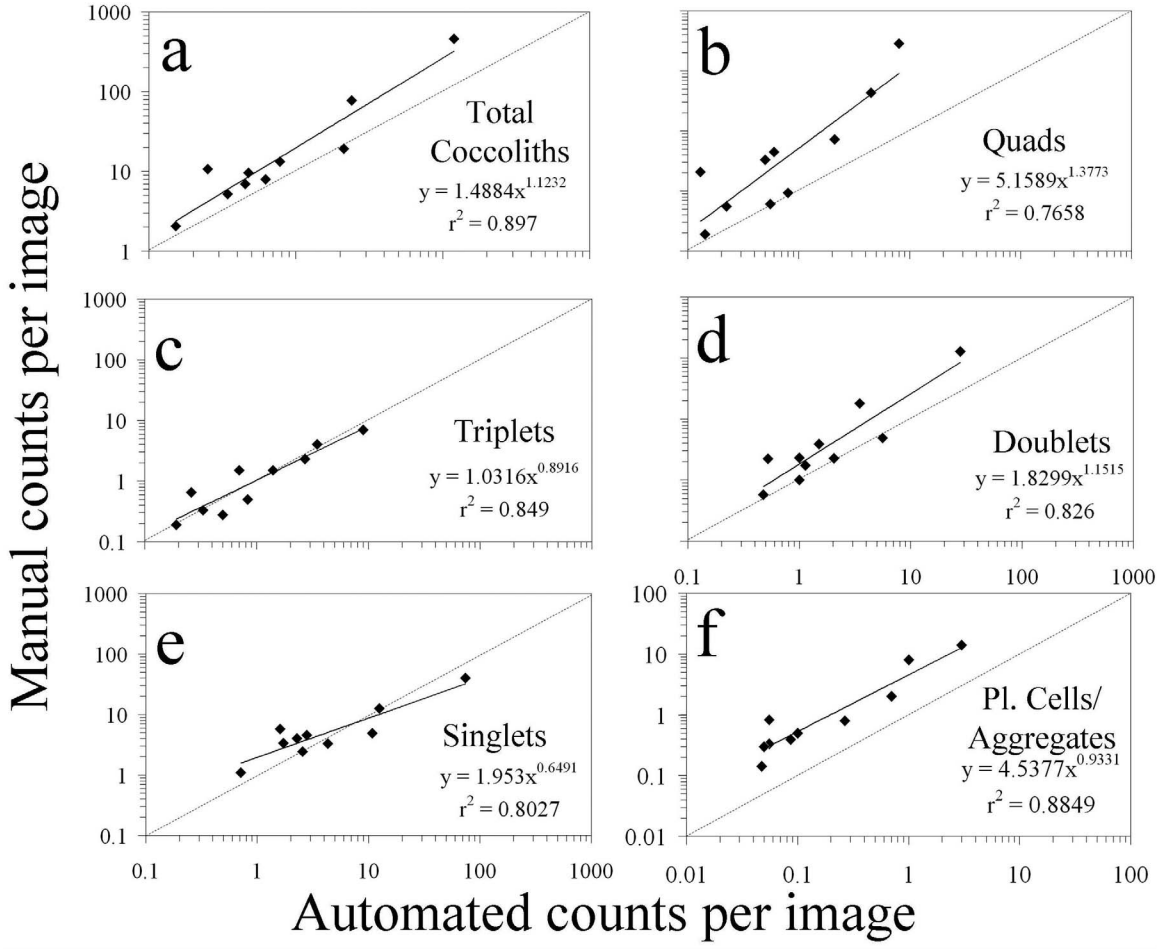

Figure 3. Performance of machine-based coccolithophore and coccolith enumeration program, CCC. The *y* axis shows manual microscope counts of particles made using the Canada Balsam technique cited in the text. The *x* axis shows CCC-derived counts made of the same slide preparations. Plots show (a) total detached coccoliths, (b) quads (coccoliths with four birefringent points of light), (c) triplets (with three birefringent points of light), (d) doublets (with two birefringent points of light), (d) singlets (with a single birefringent point of light), and (e) plated cells and aggregates. Best fit power functions and correlation coefficients are shown along with the 1:1 reference line drawn (dashed line).

concentration based on radiometric data (with the two-band/three-band merged PIC algorithm; mol m^{-3}) showed most elevated PIC concentrations in the region of the Lagrangian patch experiments and lowest concentrations south of the PF (similar to the b_b' values).

3.4. Discrete Surface Water Samples

[22] Discrete water samples were run for PIC, BSi, and coccolithophore/detached coccolith counts. PIC showed highest concentrations (peak values of 0.0005–0.001 mol m^{-3}) north of the SAF and in the region of the patch experiments

Table 1. Regression Statistics for Machine and Manual Birefringence Counts of Detached Coccoliths and Plated Coccolithophores/Coccolith Aggregates[a]

Particle Type	A	SE	B	SE	SE of Y	r^2	F	SS	SS Residual	Significance
Total coccoliths	1.488355	0.486836	1.123163	0.134551	0.225484	0.897014	69.68019	3.542739	0.406743	$P < 0.001$
Singlets	1.953058	0.424319	0.649051	0.113752	0.197376	0.802744	32.55648	1.268313	0.311659	$P < 0.001$
Doublets	1.829866	0.45481	1.15154	0.186999	0.298521	0.825788	37.92101	3.379326	0.712919	$P < 0.001$
Triplets	1.031564	0.162378	0.891634	0.132967	0.21506	0.848961	44.96643	2.079725	0.370005	$P < 0.001$
Quadruplets	5.158939	1.930319	1.377307	0.269259	0.488659	0.765842	26.16492	6.247856	1.9103	$P < 0.002$
PCCAs	4.537668	1.212454	0.933051	0.118952	0.230467	0.884938	61.52747	3.268042	0.424921	$P < 0.001$

[a]Plated coccolithophores/coccolith aggregates, PCCAs. Power function models were fit to the data in Figure 3 ($Y = AX^B$). Table presents the best fit exponent and its standard error (SE), the constant and its SE, the SE of the predicted manual count, regression squared correlation coefficient, regression F statistic, regression sum of squares (SS), residual SS, and significance. All regressions were based on 10 seawater samples (with an average ~14 images per sample). Significance level defined assuming 8 degrees of freedom for two-tailed alpha distribution.

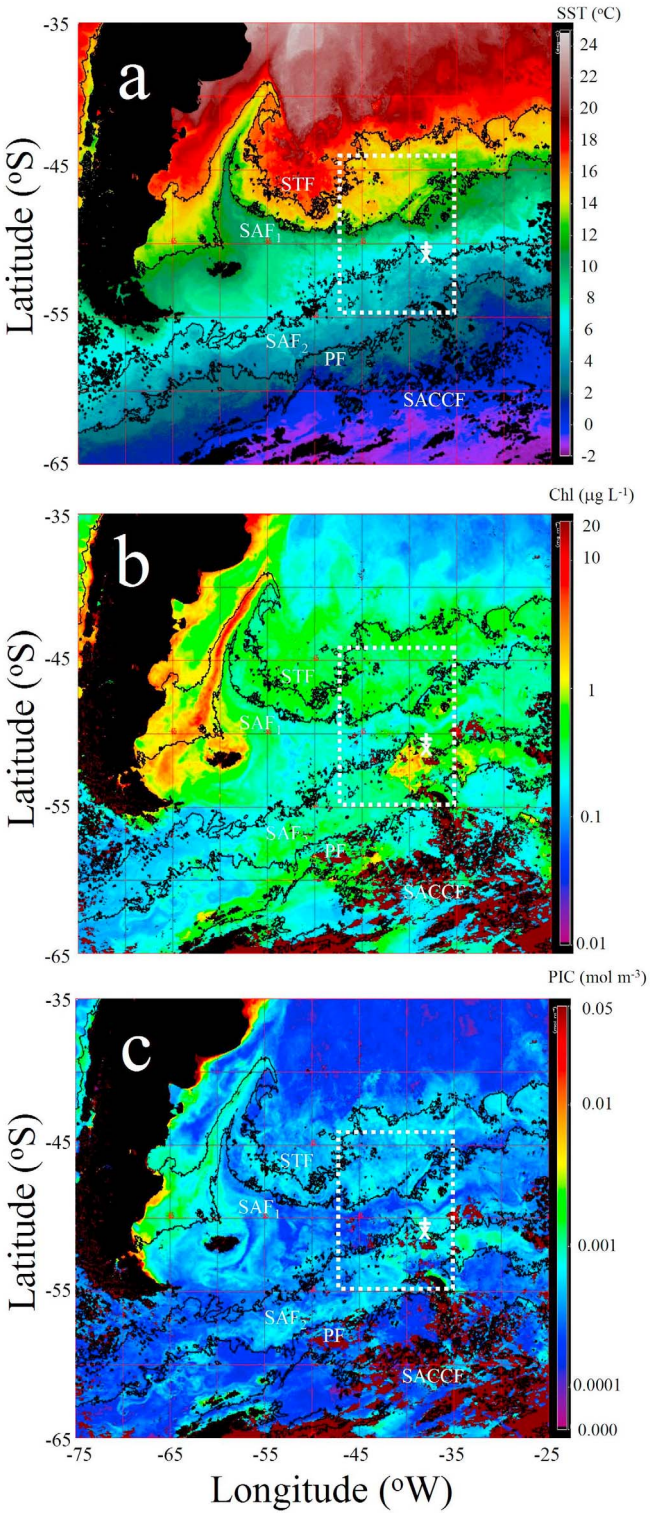

Figure 4. MODIS-Aqua imagery for the Southern Ocean (Atlantic Sector) during March 2008. (a) Sea surface temperature (SST). Frontal boundaries are marked for the Subtropical Front (STF), northern part of the Subantarctic Front (SAF_1), southern part of the Subantarctic Front (SAF_2), Polar Front (PF), and southern portion of the Antarctic Circumpolar front (SACCF) as described in the text. (b) MODIS-Aqua chlorophyll product with same frontal boundaries as marked in Figure 4a. (c) PIC product as derived by MODIS-Aqua with same frontal boundaries noted in Figure 4a. Locations of patches 1 and 2 are marked with a plus and cross, respectively. It can be seen that patch 1 was just north of SAF_2, while patch 2 was south of SAF_2. Note strong gradients in PIC and chlorophyll *a* associated with the temperature fronts.

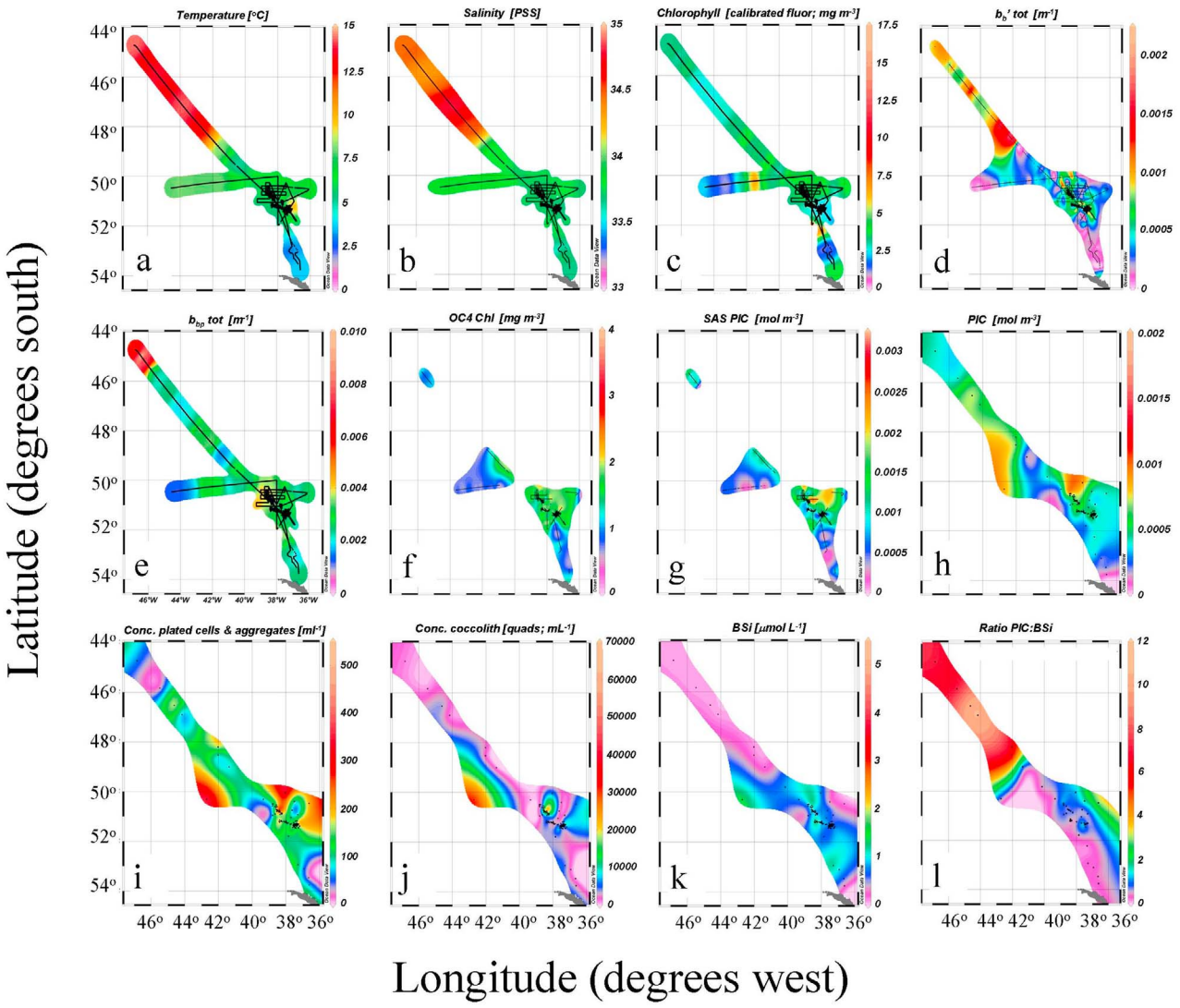

Figure 5. Surface water properties measured along track during cruise at a water depth of 2 m: (a) temperature (°C), (b) salinity (PSS), (c) chlorophyll fluorescence (calibrated to underway chlorophyll a; mg m^{-3}), (d) acid-labile backscattering (m^{-1}), (e) total particle backscattering (m^{-1}), (f) chlorophyll concentration estimated using above-water radiance data and OC-4 algorithm (mg chlorophyll *a* m^{-3}), (g) PIC concentration (mol m^{-3}) derived from above-water radiance data and merged two-band/three-band PIC algorithms [*Balch et al.*, 2005; *Gordon et al.*, 2001], (h) PIC concentration (mmol m^{-3}) as measured on discrete water samples and ICP-OES, (i) concentration of plated coccolithophores and coccolith aggregates (mL^{-1}), (j) concentration of detached quad coccoliths (mL^{-1}), (k) concentration of biogenic silica (μmol L^{-1}), and (l) molar ratio of PIC:BSi.

(Figure 5h). The concentration of plated coccolithophores and coccolith aggregates also showed patchy distributions with lowest concentrations at the extreme north and south of the study area (20–50 particles mL^{-1}). Greatest concentrations were found in the region of the experimental patches (100–400 cells mL^{-1}; Figure 5i). Detached coccolith concentrations were generally less than several hundred per mL. Exceptions to this were between the SAF and PF, where detached coccolith concentrations were 10,000–30,000 per mL (Figure 5j). Biogenic silica concentrations were low north of the SAF and showed elevated values south of the SAF, extending well south of the PF (1–2 μmol L^{-1}; Figure 5k). The ratio of PIC to BSi showed a strongly bimodal distribution, with values of either 8–10 north of the SAF and values <1 to the south (Figure 5l). The average ratios of PIC/chlorophyll and BSi/chlorophyll were 0.20 μM PIC (μg chlorophyll *a*)$^{-1}$ (standard error = ±0.010; n = 107) and 0.30 μM BSi (μg chlorophyll *a*)$^{-1}$ (standard error = ±0.015; n = 107), respectively.

3.5. Vertical Sections

[23] Due to the storm that interrupted the first Lagrangian patch experiment (after 6 days), the duration of observations is too short to see significant change, we henceforth highlight the results of the second Lagrangian experiment which lasted 13 days. Figure 6 illustrates the data taken from the

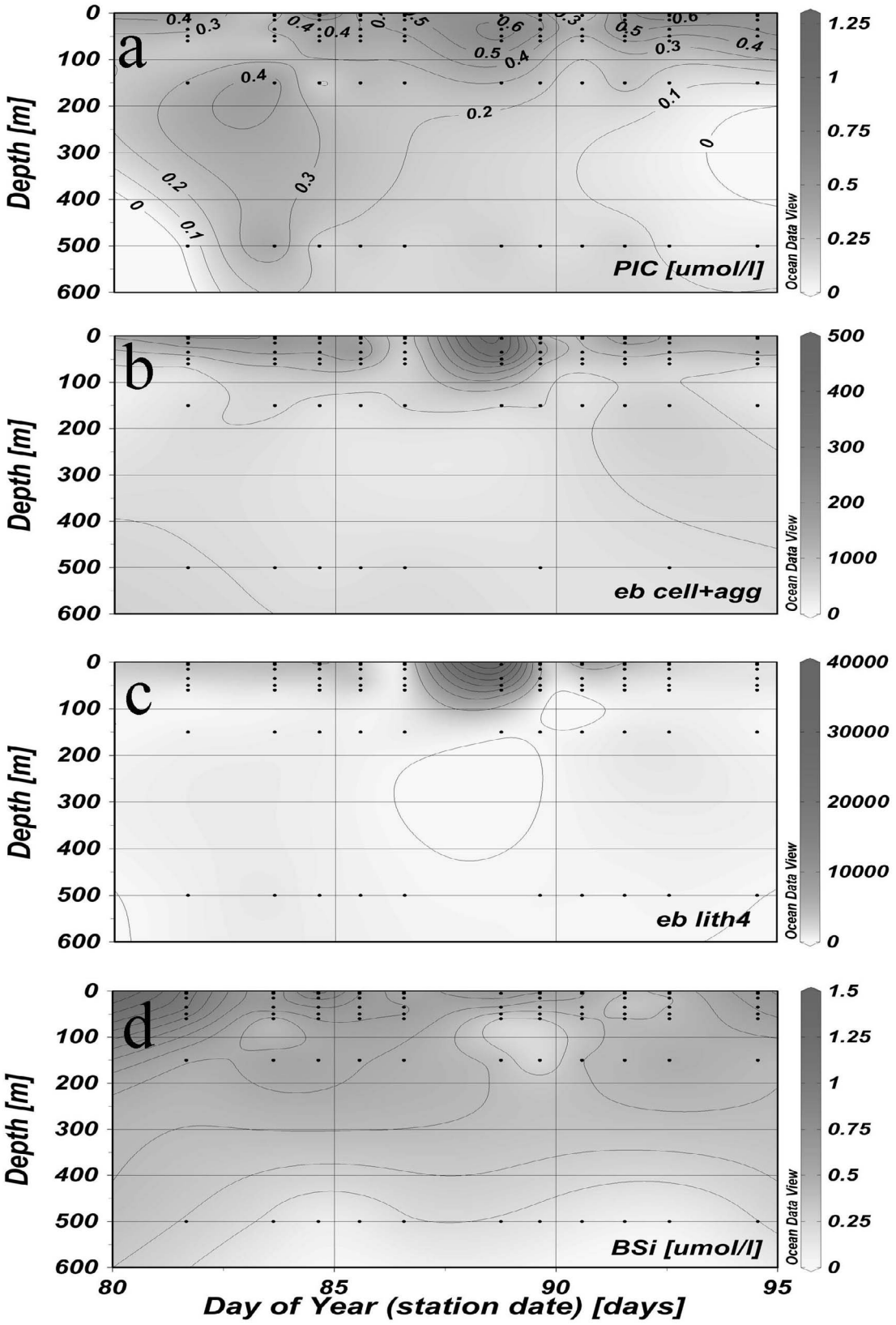

Figure 6. Time course at center of patch 2 for depth profiles of the concentration of (a) PIC (μmol L^{-1}), (b) plated coccolithophore cells and aggregates (cells mL^{-1}), (c) detached coccoliths (mL^{-1}), and (d) biogenic silica (μmol L^{-1}). Color bar given on the right and contours provided for easier interpretation.

Table 2. Results of Regressions of Integrated Mixed Layer Properties Versus Time for PIC Concentration, Coccolith Concentration, or Biogenic Silica[a]

Patch/Layer	Elapsed Time (days)	Net Δ PIC (mmol m^{-2} d^{-1})	SE	r^2	DF	Net Δ Coccoliths (mmol m^{-2} d^{-1})	SE	r^2	Net Δ BSi (mmol m^{-2} d^{-1})	SE	r^2
Patch 1 Mixed Layer (40 m)	7.7	−1.864	1.047	0.441	4	−2.17E+10	5.76E+10	0.03	−1.48	0.75	0.49
Patch 1 (500 m)	7.7	10.083	11.114	0.171	4	−6.82E+10	9.24E+10	0.15	2.64	7.57	0.03
Patch 2 Mixed Layer (50 m)	13.0	0.678	0.297	0.367[b]	9	3.27E+08	3.24E+10	0.00	−1.87	0.49	0.617[c]
Patch 2 (500 m)	13.0	−3.660	4.234	0.077	9	−1.76E+10	2.211E+10	0.07	−5.62	2.44	0.372[b]

[a]Standard error (SE) limits, regression coefficients (r^2), and degrees of freedom (DF) also given.
[b]Significance level $P < 0.1$.
[c]Significance level $P < 0.01$.

center of the second patch (located using SF6 distribution, sampled at the same time each day). PIC concentrations (μg L^{-1}; Figure 6a) showed a surface maximum in PIC in the top 100–150 m. With the exception of one datum at 500 m from day 83 (which we report but which appears to be anomalous), all other 500 m PIC data were <0.25 μmol L^{-1}. The concentration of plated coccolithophores in the middle of patch 2 were elevated in the top 150 m during the entire experiment (concentrations of 150–300 plated cells mL^{-1}), with reduced concentrations at 150 m depth (<50 mL^{-1}; Figure 6b). Spatial trends in the concentration of detached coccoliths were similar to the plated cell concentrations (with 2000–20,000 coccoliths mL^{-1} in the top 150 m and concentrations of <1000 coccoliths mL^{-1} at depths ≥500 m; Figure 6c). During day 88, there was a pronounced increase in both plated cells/aggregates and detached coccoliths, which lasted about 2 days total.

[24] Biogenic silica concentrations were also elevated in surface waters but the vertical gradients were considerably more gradual than for PIC (Figure 6d). Based on the contouring, the BSi levels were highest (>0.5 μL^{-1}) in the top 150 m with values of 0.1 μmol L^{-1} at 500 m.

3.6. Integrated Mixed Layer Changes

[25] The time series of integrated mixed layer PIC, detached coccoliths and BSi concentrations were examined within each patch (patch 1 = 40 m mixed layer and patch 2 = 50 m) or to 500 m (Table 2). Results demonstrated that there was no significant temporal trend in integrated PIC, BSi or coccolith concentration within patch 1, for integrals over the mixed layer or 500 m. For patch 2, however, there was a significant ($P < 0.01$) decrease in mixed layer BSi over the 13 days, with a mean trend of −1.875 mmol m^{-1} d^{-1}. Moreover, there was an increase in mixed layer PIC for the same patch (mean trend = 0.68 mmol m^{-1} d^{-1}), although this change was not significant at the 0.05% alpha level ($P < 0.1$; Table 2 and Figure 7). When integrated to 500 m, the only significant trend for patch 2 was a negative one for BSi ($P < 0.1$; Table 2). Integrated mixed layer concentrations of coccoliths and plated coccolithophores in patch 2 showed increasing concentrations, peaking on day 7 after which the concentrations declined (results not shown).

4. Discussion

4.1. Automated Coccolithophore Enumeration

[26] Coccolith and coccolithophore counts made with CCC software were significantly correlated to manual counts but with varying degrees of bias. In virtually all the cases, manual counts were higher than the machine counts (Figure 3) except for counting birefringent "triplets" or "singlets," which were not significantly different from each other. Neural network approaches for enumerating coccoliths/coccolithophores have been used before [*Beaufort*, 2005; *Beaufort and Dollfus*, 2004]. Indeed, they, too, have shown biases, with higher concentrations observed in manual counts than machine counts, by about a factor of 2 [*Beaufort and Dollfus*, 2004]. CCC, unlike the neural network approach, only classifies birefringent coccoliths and coccolithophores and provides no taxonomic information, just presence or absence as well as size. It could be adapted to discriminate birefringent pattern, provided that unique birefringent patterns could be distinguished. In both cases, manual versus machine biases can be compensated for using the calibration curves, such as those shown in Figure 3. A limitation of CCC for enumerating coccoliths (or any birefringence-based technique) is that some noncalcium carbonate particles are birefringent. Indeed, the ocean contains a wide variety of such particles, one of the most common being certain dinoflagellate thecae [*Balch and Fabry*, 2008]. This would tend to make measurements based purely on the *amount* of birefringence light per particle an overestimate of the mass of PIC. In CCC however, particles like dinoflagellate thecae, that do not have a birefringence pattern like a coccolith or plated coccolithophore will not be enumerated.

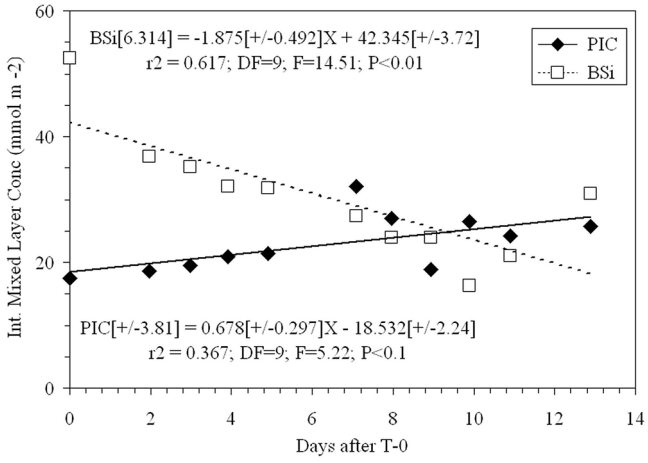

Figure 7. Integrated mixed layer concentrations of PIC (solid diamonds) and BSi (open squares), measured at the center of patch 2. Best fit linear fit equations along with associated statistics are shown.

4.2. SO GasEx Observations Consistent With the Great Calcite Belt Hypothesis

[27] The evidence presented here and elsewhere suggests that the high reflectance in the vicinity of the GasEx site was due, at least partially, to coccolithophores and their detached coccoliths. Indeed, there was evidence from the SO GasEx experiments (based on the unique volume scattering of bubbles at 83°) that bubbles were a source of enhanced reflectance (Randolph et al., submitted manuscript, 2011). However, evidence presented here suggests that coccoliths also played a critical role in enhancing the reflectance from Southern Ocean waters. Certainly, the coccolithophore counts (with coccolith concentrations >20,000 mL^{-1} and plated cell concentrations >400 mL^{-1}), with stable (or increasing) concentrations over the 13 day occupation of the second patch, was ample proof of their presence and stability. Such concentrations would have approximately doubled the water-leaving radiance at 550 nm, at the observed concentration of chlorophyll *a* [see *Balch et al.*, 2005, Figure 3]. Our underway optical results also demonstrated high levels of acid-labile backscattering, consistent with elevated PIC concentrations, regardless of sea state (as opposed to enhanced bubbles, which would have been reduced in quiescent conditions and elevated during storm events). This rationale also worked in the converse situation, when winds and sea states were high and PIC concentrations were low, above-water reflectance measurements showed low overall PIC concentrations (Figures 5g and 5h). For example, when the R/V *Ron Brown* traveled to South Georgia Island for shelter from a powerful storm, the data from the bow-mounted MicroSAS demonstrated a strong decline in reflectance, commensurate with the decline in PIC levels south of the Polar Front, despite the fact that winds and sea states were elevated.

[28] Thus, there was generally good (but not exact) correspondence between the regional trends in the analytical PIC measurements (Figure 5h) and the radiometrically derived PIC values determined with the SAS (Figure 5g). But note, when compared in common units, the ratio of SAS-derived PIC: analytical PIC averaged about 3.05 (standard error = ±0.39; n = 30; median = 2.43), which well may have occurred due to the presence of small bubbles (at least on windy days) thus increasing the 550 nm reflectance. Nonetheless, our standard practice for processing SAS-derived PIC values is to only accept the lowest 5% of the radiances, precisely to remove white cap and foam contaminated waters. While this should have minimized the effect of bubbles, it is certainly plausible that small bubbles with long residence times might not have been removed by such filtering.

4.3. Integrating Results Over Basin Scales: More Evidence for the Great Calcite Belt

[29] Indeed, our results fit a pattern of elevated coccolith PIC, part of a much larger feature that actually encircles the globe. Based on MODIS-Aqua satellite ocean color during the SO GasEx expedition as well as optical data from five other cruises (see Figure 1 and *Balch and Utgoff* [2009]), the high-reflectance water in the Southern Ocean occurred along the SAF and PF of the Atlantic sector, whether the winds were high or not. This adds further evidence on the importance of coccolithophores to the total scattering since it is common for unique phytoplankton (as opposed to bubbles) to be associated with hydrographic fronts [*Holligan et al.*, 1983a, 1983b]. The appearance of this high-reflectance feature in the Southern Ocean in the austral summer is fully consistent with a coccolithophore source, too, given the tendency of coccolithophores to bloom during summer months, near the summer solstice [*Balch*, 2004].

[30] During the past several years, other workers have observed coccolithophore features near the same frontal boundaries in the Southern Ocean. *Cubillos et al.* [2007] sampled a transect between Tasmania and Antarctica (43°S–60°S) in 2005–2006 and observed plated *E. huxleyi* cell concentrations of several hundred per mL, with enhanced concentrations in both the Subantarctic and Polar Frontal zones. They also observed an increasing presence of the *E. huxleyi* coccolith morphology type B/C south of the PF as well as clear evidence of dissolution. *Gravalosa et al.* [2008] performed an intensive zonal transect in the Pacific sector of the Southern Ocean (90°W–120°W) along the Subantarctic Front (~56°S), as well as a meridional transect crossing the SAF, PF and the southern front of the ACC (between 57°S and 60°S along ~115°W–117°W). They documented total plated coccolithophore concentrations (of *E. huxleyi* and *Calcidiscus leptoporus*) up to 180 cells mL^{-1} with peaks within the SAF and PF. Typically, for *E. huxleyi*, detached coccolith concentrations are at least 15–20X the concentration of plated cells [*Balch et al.*, 1993] (which would represent ~2700 mL^{-1}) which would only slightly enhance satellite reflectance [*Balch et al.*, 2005]. *Holligan et al.* [2010] measured coccolithophore concentrations across the Drake Passage and observed coccolith concentrations up to 30,000 mL^{-1} and PIC concentrations up to 1.2 μM, which would significantly enhance the water-leaving reflectance from such waters. In the Indian sector of the Southern Ocean (45°E), *Mohan et al.* [2008] observed highest concentrations (~400 cells mL^{-1}) of *E. huxleyi* associated with the STF, SAF and PF, with decreasing taxonomic diversity trending southward. They also noted different *E. huxleyi* morphotypes at these frontal boundaries.

[31] It is worthy of note that our evidence presented here, along with the other references [*Cubillos et al.*, 2007; *Gravalosa et al.*, 2008; *Holligan et al.*, 2010; *Mohan et al.*, 2008], suggests that this region of enhanced coccolithophore concentrations is limited in its southern extent to the PF. During our transect to S. Georgia Island during the SO GasEx experiment, acid-labile backscattering dropped to almost zero at about 52°S (Figure 5d). *Mohan et al.* [2008] saw a dramatic decline in *E. huxleyi* abundance at 47°S with a change in coccolith morphology from B/C to D. Surface abundances were low (but still measureable) to 54°S. *Holligan et al.* [2010] observed the dramatic dropoff at about 54°S in the Drake Passage. *Gravalosa et al.* [2008] and *Cubillos et al.* [2007] in the Pacific sectors observed this decrease southward of 60°S. *Cubillos et al.* [2007] based on cruises spanning decades (1983–2006) suggests that *E. huxleyi* has been increasing its southward range over the past several decades, just as others have conjectured in Arctic waters [*Smyth et al.*, 2004]. In summary, our results indeed, support the existence of a circumpolar region of elevated PIC which we refer to as the Great Calcite Belt.

4.4. A Dramatic Switch in Biominerals Across the SAF

[32] One of the most striking biogeochemical changes noted in the study area during SO GasEx was the shift from mostly coccolithophore PIC just north of the patch site, near SAF_1, to diatom BSi south of SAF_1 with an order of magnitude gradient (Figure 5l). These results provide some insight into what sets the southern boundary of the Great Calcite Belt. Ironically, the absolute abundance of coccolithophores, their detached coccoliths plus PIC concentrations, and b_b' values were all high north of SAF_1 (near the study site) but clearly the diatoms responded with bigger increases south of SAF_1 than did the coccolithophores. It was not until south of the PF (52°S) when the absolute abundance of coccolithophores dropped significantly, consistent with patterns in water-leaving radiance observed by satellite.

[33] Careful examination of satellite imagery (Figure 4) reveals that chlorophyll and PIC were elevated between (1) the STF and SAF_1 and (2) the SAF_2 and PF, with low chlorophyll *a* and PIC concentrations between the SAF_1 and SAF_2. Meridional sections of nutrients [*Tsuchiya et al.*, 1994] provide some insight into this distribution. Isopleths of nitrate, silicate and phosphate all deepen more between SAF_1 and SAF_2 than they do between STF and SAF_1 or SAF_2 and the PF. Hence, a bottom-up, nutrient supply mechanism seems the most reasonable to explain the patterns of chlorophyll *a* and PIC, as observed in the MODIS-Aqua imagery. On a broader scale, the southward shoaling of water with silicate levels >2 μM, south of SAF_1 [see *Tsuchiya et al.*, 1994, Figure 6] can explain the overall shift from carbonate-dominated waters to BSi-dominated waters to the south (Figure 5l).

[34] The actual nutrient concentrations (V. P. Lance et al., Primary productivity, new productivity and carbon export during two Southern Ocean Gas Exchange (SO GasEx) tracer experiments, unpublished manuscript, 2011) measured in the mixed layer of both patches resembled high-nutrient low-chlorophyll waters [*Minas and Minas*, 1992; *Minas et al.*, 1986], with nitrate concentrations of 14–18 μM, NH_4^+ concentrations of 1–2 μM, PO_4 concentrations 1–1.2 μM and $Si(OH)_4$ concentrations of <1–3 uM. Ratios of dissolved inorganic nitrogen to phosphate were close to, or slightly below, Redfield values of 16. Moreover, silicate to nitrate ratios were extremely low (patch 1 = 0.05; patch 2 = 0.2) suggesting that diatom growth was strongly limited by Si at the patch sites. Thus, the moderate levels of coccolithophores found at the patch sites were not related to phosphorous limitation as suggested in the Introduction but may have been due to a competitive advantage over diatoms in the silica-limited waters.

[35] When the PIC concentration in seawater is normalized by the concentration of detached coccoliths (including a correction for the attached coccoliths), the PIC per coccolith typically varied between about 0.3 and 60 pg/coccolith [*Balch et al.*, 2000]. The large range is likely due to other noncoccolith $CaCO_3$ particles captured during filtration that increase the value from what has been reported for pure *E. huxleyi* cultures or relatively pure *E. huxleyi* blooms (0.06–0.6 pg coccolith^{-1} [*Balch et al.*, 1996]). In SO GasEx, the average PIC per coccolith was 0.83 pg coccolith^{-1} (standard error = ±0.080; n = 107), higher than expected for *E. huxleyi* but no data are available for other coccolithophore species in the assemblage. Given the proximity of the study site to the SAF, then the most likely species present would have been *E. huxleyi* and *Calcidiscus leptoporus*, the latter being a coccolithophore species with larger, heavier coccoliths than *E. huxleyi* [*Gravalosa et al.*, 2008; *Mohan et al.*, 2008; *Winter and Siesser*, 1994]. It is also worthy of note that our results demonstrated no statistically significant relationships in the PIC per cell as a function of latitude or temperature, in contrast to *Holligan et al.* [2010]. Nonetheless, the average biogeochemical ratios, PIC/chlorophyll and BSi/chlorophyll, were about the same as those reported by *Holligan et al.* [2010] for the SAF suggesting similar relative quantities of coccolithophores and diatoms within the phytoplankton community.

4.5. Loss of PIC and BSi From the Surface Layer at the SAF

[36] PIC and coccolithophore abundance data demonstrated clear decreases in concentrations below the 80 m isobath (Figure 6) suggestive of rapid turnover. A possible reason for this decrease could have been zooplankton grazing and repackaging of PIC into fast sinking fecal pellets. Alternatively, it may have resulted from supralysocline dissolution associated with grazing and bacterial remineralization [*Milliman et al.*, 1999]. Carbonate ion concentrations are still considered to be supersaturated in the upper 500 m of the ACC region (50°S–70°S) for both calcite or aragonite, but values are close to saturation for aragonite within the top few hundred meters for all three sectors of the Southern Ocean [*Feely et al.*, 2009]. We note that this vertical loss of PIC existed in a period of net calcification at the patch site (in which integrated PIC was increasing by about 2% d^{-1}; Figure 7) with an overall minor increase in concentration of 7 mmol m^{-2} over the 13 days that patch 2 was occupied. This change was barely significant ($P < 0.1$). Interestingly, changes in alkalinity observed by T. S. Moore et al. (Sea surface pCO2 and O2 in the Southern Ocean during the austral fall 2008, submitted to *Journal of Geophysical Research*, 2011) in patch 2 were about +0.62 μmol kg^{-1} d^{-1}, barely measurable, qualitatively consistent with the low calcification rates that we estimated here.

[37] Recall that the vertical distribution of BSi also showed pronounced decreases, but between 150 and 500 m, deeper than the disappearance horizon for PIC. If the same grazing/repackaging was responsible for these changes as for PIC, then the disappearance horizon for BSi would have been expected to be similar (or shallower) than PIC, especially since it was showing net *decreases* over time whereas PIC was increasing (Figure 7). On average, 50–60% of the BSi dissolves in the upper 100 m of the ocean [*Nelson et al.*, 1995; *Van Cappellen et al.*, 2002]. The rate of loss in BSi in the Lagrangian patch was about half of the mean rates measured in the Southern Ocean (5.33 ± 3.81 mmol m^{-2} d^{-1}) [*Brzezinski et al.*, 2001] and close to the mean value cited for a more temperate location, Monterey Bay (2.9 mmol m^{-2} d^{-1}) [*Brzezinski et al.*, 2003]). Surface silicate concentrations rose within this patch by about 2 mmol m^{-3} over the 13 days that patch 2 was followed. Integrated over the top 50 m mixed layer, this translated to a silicate increase of 100 mmol m^{-2} (M. D. Degrandpre and T. S. Moore, personal communication, 2010) compared to the integrated decrease in BSi of about 20 mmol m^{-2}. Thus, remineralization of BSi could have

only contributed 20% of the net increase of silicate, the remainder which must have been associated with other sources such as lateral advection (despite the fact that the patches were followed using Lagrangian-advected SF_6, steady changes in nutrients over stable water columns suggest non-Lagrangian behavior of the patch with lateral intrusions).

4.6. Concluding Remarks

[38] Our results from SO GasEx demonstrate a region of elevated coccolithophorid populations near the SAF. Evidence for sustained, elevated coccolithophore concentrations came from microscopy, analytical PIC measurements as well as acid-labile backscattering measurements and above water measurements of apparent optical properties (from ship and satellite). This time series of intensive measurements of sustained enhanced PIC at one location within the SAF (a first) showed results in agreement with other published observations from this frontal region in the different sectors of the Southern Ocean, consistent with the hypothesis that the SO GasEx site was part of a larger region of enhanced PIC encircling the Southern Ocean, an area we here call the Great Calcite Belt. MODIS-Aqua and SeaWiFS imagery taken over the past one and a half decades in the Southern Ocean consistently show such high reflectance during the Austral summers. The reflectance per unit PIC was greater than has been measured before. We would attribute this to other hypothesized sources of backscattering in this region, such as bubble injection, at least during intense wind and wave energy events (see Randolph et al., submitted manuscript, 2011). The hypothesized Great Calcite Belt covers a large area of the global ocean (some 88 million km^2, or 16% of the world ocean). The biogeochemical impact of this feature is not well understood. Future cruises are being performed to assess the importance of this region to the DIC cycle as well as the overall biogeochemical cycle and biological carbon pump.

[39] **Acknowledgments.** We dedicate this work to the late Paul Utgoff (Professor, Computer Science Department, University of Massachusetts, Amherst, Massachusetts) who was instrumental in developing the CCC software used here for automated enumeration of coccolithophorids and detached coccoliths. Because of his untimely death in October 2008, he unfortunately never saw the the application of CCC to a real oceanographic problem. Heidi Diersson provided superb leadership in running of this project. We wish to thank David Ho and Chris Sabine (cochief scientists) for leading the SO GasEx cruise effort. C. Del Castillo and R. Miller (NASA) provided considerable help at sea. Veronica Lance (LDEO) aided with processing the many chlorophyll samples and provided background on the nutrient distributions at the patch site. Quincy Allison (NASA, AMES) provided expert logistical support for getting equipment to and from the ship. Michael DeGrandpre and Tommy Moore (University of Montana) helped reconcile our observed changes in biogenic silica and calcification relative with their observed changes in silicate and alkalinity, respectively. We also would like to thank the crew of the R/V *Ron Brown* for their assistance in sampling under difficult conditions. Ocean Data View software (R. Schlitzer, http://odv.awi.de, 2007) was used to generate the plots in Figures 2, 5, and 6. We gratefully acknowledge the support by the National Aeronautic and Space Administration (contracts NNX08AB10G, NNX07AD01G, NNX08AJ88A, and NNX10AT67G). The National Science Foundation provided support for development of the CCC software used to enumerate coccolithophores (OCE-0325937) as well as other funds for studying the Great Calcite Belt (OCE-0961660 and OCE-0728582).

References

Armstrong, R. A., C. Lee, J. I. Hedges, S. Honjo, and S. G. Wakeham (2001), A new, mechanistic model for organic carbon fluxes in the ocean based on the quantitative association of POC with ballast minerals, *Deep Sea Res. Part II*, *49*, 219–236, doi:10.1016/S0967-0645(01)00101-1.

Balch, W. M. (2004), Re-evaluation of the physiological ecology of coccolithophores, in *Coccolithophores: From Molecular Processes to Global Impact*, edited by H. R. Thierstein and J. R. Young, pp. 165–190, Springer, Berlin.

Balch, W. M., and V. J. Fabry (2008), Ocean acidification: Documenting its impact on calcifying phytoplankton at basin scales, *Mar. Ecol. Prog. Ser.*, *373*, 239–247, doi:10.3354/meps07801.

Balch, W. M., and P. E. Utgoff (2009), Potential interactions among ocean acidification, coccolithophores and the optical properties of seawater, *Oceanography*, *22*, 146–159.

Balch, W. M., P. M. Holligan, S. G. Ackleson, and K. J. Voss (1991), Biological and optical properties of mesoscale coccolithophore blooms in the Gulf of Maine, *Limnol. Oceanogr.*, *36*, 629–643, doi:10.4319/lo.1991.36.4.0629.

Balch, W. M., K. A. Kilpatrick, and P. M. Holligan (1993), Coccolith formation and detachment by *Emiliania huxleyi* (Prymnesiophyceae), *J. Phycol.*, *29*, 566–575, doi:10.1111/j.0022-3646.1993.00566.x.

Balch, W. M., K. Kilpatrick, P. M. Holligan, D. Harbour, and E. Fernandez (1996), The 1991 coccolithophore bloom in the central north Atlantic. Part II. Relating optics to coccolith concentration, *Limnol. Oceanogr.*, *41*, 1684–1696, doi:10.4319/lo.1996.41.8.1684.

Balch, W. M., D. Drapeau, and J. Fritz (2000), Monsoonal forcing of calcification in the Arabian Sea, *Deep Sea Res. Part II*, *47*, 1301–1337, doi:10.1016/S0967-0645(99)00145-9.

Balch, W. M., D. Drapeau, J. Fritz, B. Bowler, and J. Nolan (2001), Optical backscattering in the Arabian Sea—Continuous underway measurements of particulate inorganic and organic carbon, *Deep Sea Res. Part I*, *48*, 2423–2452, doi:10.1016/S0967-0637(01)00025-5.

Balch, W. M., H. R. Gordon, B. C. Bowler, D. T. Drapeau, and E. S. Booth (2005), Calcium carbonate budgets in the surface global ocean based on MODIS data, *J. Geophys. Res.*, *110*, C07001, doi:10.1029/2004JC002560.

Balch, W. M., B. C. Bowler, D. T. Drapeau, A. Poulton, and P. Holligan (2010), Biominerals and the vertical flux of particulate organic carbon from the surface ocean, *Geophys. Res. Lett.*, *37*, L22605, doi:10.1029/2010GL044640.

Beaufort, L. (2005), Weight estimates of coccoliths using the optical properties (birefringence) of calcite, *Micropaleontology*, *51*, 289–297, doi:10.2113/gsmicropal.51.4.289.

Beaufort, L., and D. Dollfus (2004), Automatic recognition of coccoliths by dynamical neural networks, *Mar. Micropaleontol.*, *51*, 57–73, doi:10.1016/j.marmicro.2003.09.003.

Broerse, A. T. C., T. Tyrrell, J. R. Young, A. J. Poulton, A. Merico, W. M. Balch, and P. I. Miller (2003), The cause of bright waters in the Bering Sea in winter, *Cont. Shelf Res.*, *23*, 1579–1596, doi:10.1016/j.csr.2003.07.001.

Brown, C. W., and J. A. Yoder (1994), Coccolithophorid blooms in the global ocean, *J. Geophys. Res.*, *99*, 7467–7482, doi:10.1029/93JC02156.

Brzezinski, M. A., and D. M. Nelson (1989), Seasonal changes in the silicon cycle within a Gulf Stream warm-core ring, *Deep Sea Res. Part I*, *36*, 1009–1030, doi:10.1016/0198-0149(89)90075-7.

Brzezinski, M. A., D. M. Nelson, V. M. Franck, and D. E. Sigmon (2001), Silicon dynamics within an intense open-ocean diatom bloom in the Pacific sector of the Southern Ocean, *Deep Sea Res. Part II*, *48*, 3997–4018, doi:10.1016/S0967-0645(01)00078-9.

Brzezinski, M. A., J. L. Jones, K. D. Bidle, and F. Azam (2003), The balance between silica production and silica dissolution in the sea: Insights from Monterey Bay, California, applied to the global data set, *Limnol. Oceanogr.*, *48*, 1846–1854, doi:10.4319/lo.2003.48.5.1846.

Cubillos, J. C., S. W. Wright, G. Nash, M. F. De Salas, B. Griffiths, B. Tilbrook, A. Poisson, and G. M. Hallegraeff (2007), Calcification morphotypes of the coccolithophorid *Emiliania huxleyi* in the Southern Ocean: Changes in 2001 to 2006 compared to historical data, *Mar. Ecol. Prog. Ser.*, *348*, 47–54, doi:10.3354/meps07058.

Feely, R., S. C. Doney, and S. R. Cooley (2009), Ocean acidification: Present conditions and future changes in a high-CO_2 world, *Oceanography*, *22*, 36–47.

Francois, R., S. Honjo, R. Krishfield, and S. Manganini (2002), Factors controlling the flux of organic carbon to the bathypelagic zone of the ocean, *Global Biogeochem. Cycles*, *16*(4), 1087, doi:10.1029/2001GB001722.

Gordon, H. R., G. C. Boynton, W. M. Balch, S. B. Groom, D. S. Harbour, and T. J. Smyth (2001), Retrieval of coccolithophore calcite concentration from SeaWiFS imagery, *Geophys. Res. Lett.*, *28*, 1587–1590, doi:10.1029/2000GL012025.

Gravalosa, J. M., J.-A. Flores, F. J. Sierro, and R. Gersonde (2008), Sea surface distribution of coccolithophores in the eastern Pacific sector of

the Southern Ocean (Bellingshausen and Amundsen Seas) during the late austral summer of 2001, *Mar. Micropaleontol.*, *69*, 16–25, doi:10.1016/j.marmicro.2007.11.006.

Gregg, W. W., and N. W. Casey (2007), Modeling coccolithophores in the global oceans, *Deep Sea Res. Part II*, *54*, 1–27, doi:10.1016/j.dsr2.2006.12.007.

Haidar, A. T., and H. R. Thierstein (2001), Coccolithophore dynamics off Bermuda (N. Atlantic), *Deep Sea Res.*, *48*, 1925–1956, doi:10.1016/S0967-0645(00)00169-7.

Ho, D. T., C. L. Sabine, D. Hebert, D. S. Ullman, R. Wanninkhof, R. C. Hamme, P. G. Strutton, B. Hales, J. B. Edson, and B. R. Hargreaves (2011), Southern Ocean Gas Exchange Experiment: Setting the stage, *J. Geophys. Res.*, doi:10.1029/2010JC006852, in press.

Holligan, P. M., M. Viollier, C. Dupouy, and J. Aiken (1983a), Satellite studies on the distributions of chlorophyll and dinoflagellate blooms in the western English Channel, *Cont. Shelf Res.*, *2*, 81–96, doi:10.1016/0278-4343(83)90009-2.

Holligan, P. M., M. Viollier, D. S. Harbout, P. Camus, and M. Champagne-Philippe (1983b), Satellite and ship studies of coccolithophore production along a continental shelf edge, *Nature*, *304*, 339–342, doi:10.1038/304339a0.

Holligan, P. M., et al. (1993), A biogeochemical study of the coccolithophore, *Emiliania huxleyi*, in the north Atlantic, *Global Biogeochem. Cycles*, *7*, 879–900, doi:10.1029/93GB01731.

Holligan, P. M., A. Charalampopoulou, and R. Hutson (2010), Seasonal distributions of the coccolithophore, *Emiliania huxleyi*, and of particulate inorganic carbon in surface waters of the Scotia Sea, *J. Mar. Syst.*, *82*, 195–205, doi:10.1016/j.jmarsys.2010.05.007.

Iida, T., S. I. Saitoh, T. Miyamura, M. Toratani, H. Fukushima, and N. Shiga (2002), Temporal and spatial variability of coccolithophore blooms in the eastern Bering Sea, 1998–2001, *Prog. Oceanogr.*, *55*, 165–175, doi:10.1016/S0079-6611(02)00076-9.

Klaas, C., and D. E. Archer (2002), Association of sinking organic matter with various types of mineral ballast in the deep sea: Implications for the rain ratio, *Global Biogeochem. Cycles*, *16*(4), 1116, doi:10.1029/2001GB001765.

Lessard, E., A. Merico, and T. Tyrrell (2005), Nitrate:phosphate ratios and *Emiliania huxleyi* blooms, *Limnol. Oceanogr.*, *50*, 1020–1024, doi:10.4319/lo.2005.50.3.1020.

Merico, A., T. Tyrrell, E. Lessard, T. Oguz, P. Stabeno, S. Zeeman, and T. Whitledge (2004), Modelling phytoplankton succession on the Bering Sea shelf: Role of climate influences and trophic interactions in generating *Emiliania huxleyi* blooms 1997–2000, *Deep Sea Res.*, *151*, 1803–1826, doi:10.1016/j.dsr.2004.07.003.

Milliman, J., P. J. Troy, W. Balch, A. K. Adams, Y.-H. Li, and F. T. MacKenzie (1999), Biologically mediated dissolution of calcium carbonate above the chemical lysocline?, *Deep Sea Res. Part I*, *46*, 1653–1669, doi:10.1016/S0967-0637(99)00034-5.

Minas, H. J., and M. Minas (1992), Net community production in "high nutrient-low chlorophyll" waters of the tropical and Antarctic oceans: Grazing vs iron hypothesis, *Oceanol. Acta*, *15*, 145–162.

Minas, H. J., M. Minas, and T. T. Packard (1986), Productivity in upwelling areas deduced from hydrographic and chemical fields, *Limnol. Oceanogr.*, *31*, 1182–1206, doi:10.4319/lo.1986.31.6.1182.

Mohan, R., L. P. Mergulhao, M. V. S. Guptha, A. Rajakumar, M. Thamban, N. AnilKumar, M. Sudhakar, and R. Ravindra (2008), Ecology of coccolithophores in the Indian sector of the Southern Ocean, *Mar. Micropaleontol.*, *67*, 30–45, doi:10.1016/j.marmicro.2007.08.005.

Mueller, J. L., et al. (2003), *Radiometric Measurements and Data Analysis Protocols*, vol. III, 78 pp., Goddard Space Flight Center, Greenbelt, Md.

Nelson, D. M., P. Treguer, M. A. Brzezinski, A. Leynaert, and B. Queguiner (1995), Production and dissolution of biogenic silica in the ocean: Revised global estimates, comparison with regional data and relationship to biogenic sedimentation, *Global Biogeochem. Cycles*, *9*, 359–372, doi:10.1029/95GB01070.

Paasche, E., and S. Brubak (1994), Enhanced calcification in the coccolithophorid *Emiliania huxleyi* (Haptophyceae) under phosphorus limitation, *Phycologia*, *33*, 324–330, doi:10.2216/i0031-8884-33-5-324.1.

Poulton, A. J., R. Sanders, P. M. Holligan, T. Adey, M. Stinchcombe, L. Brown, and K. Chamberlain (2006), Phytoplankton mineralisation in the tropical and subtropical Atlantic Ocean, *Global Biogeochem. Cycles*, *20*, GB4002, doi:10.1029/2006GB002712.

Riegman, R., A. Noordeloos, and G. Cadee (1992), Phaeocystis blooms and eutrophication of the continental coastal zones of the North Sea, *Mar. Biol.*, *112*, 479–484, doi:10.1007/BF00356293.

Riegman, R., W. Stolte, A. Noordeloos, and D. Slezak (2000), Nutrient uptake and alkaline phosphatase (EC 3:1:3:1) activity of *Emiliania huxleyi* (Prymnesiophyceae) during growth under N and P limitation in continuous cultures, *J. Phycol.*, *36*, 87–96, doi:10.1046/j.1529-8817.2000.99023.x.

Satoh, M., K. Iwamoto, I. Suzuki, and Y. Shiraiwa (2009), Cold stress stimulates intracellular calcification by the coccolithophore, *Emiliania huxleyi* (Haptophyceae) under phosphate-deficient conditions, *Mar. Biotechnol.*, *11*, 327–333, doi:10.1007/s10126-008-9147-0.

Smyth, T. J., T. Tyrrell, and B. Tarrant (2004), Time series of coccolithophore activity in the Barents Sea, from twenty years of satellite imagery, *Geophys. Res. Lett.*, *31*, L11302, doi:10.1029/2004GL019735.

Townsend, D. W., M. D. Keller, P. M. Holligan, S. G. Ackleson, and W. M. Balch (1994), Blooms of the coccolithophore *Emiliania huxleyi* with respect to hydrography in the Gulf of Maine, *Cont. Shelf Res.*, *14*, 979–1000, doi:10.1016/0278-4343(94)90060-4.

Tsuchiya, M., L. D. Talley, and M. S. McCartney (1994), Water-mass distributions in the western South Atlantic: A section from South Georgia Island (54S) northward across the equator, *J. Mar. Syst.*, *52*, 55–81.

Tyrrell, T., and A. Merico (2004), *Emiliania huxleyi*: Bloom observations and the conditions that induce them, in *Coccolithophores: From Molecular Processes to Global Impact*, edited by H. R. Thierstein and J. R. Young, pp. 75–97, Springer, Berlin.

Tyrrell, T., and A. H. Taylor (1995), Latitudinal and seasonal variations in carbon dioxide and oxygen in the northeast Atlantic and the effects on *Emiliania huxleyi* and other phytoplankton, *Global Biogeochem. Cycles*, *9*, 585–604, doi:10.1029/95GB01133.

Tyrrell, T., and A. H. Taylor (1996), A modelling study of *Emiliania huxleyi* in the NE Atlantic, *J. Mar. Syst.*, *9*, 83–112, doi:10.1016/0924-7963(96)00019-X.

Van Cappellen, P. V., S. Dixit, and J. van Beusekom (2002), Biogenic silica dissolution in the oceans: Reconciling experimental and field-based dissolution rates, *Global Biogeochem. Cycles*, *16*(4), 1075, doi:10.1029/2001GB001431.

Wal, P. d., R. S. Kempers, and M. J. W. Veldhuis (1995), Production and downward flux of organic matter and calcite in a North Sea bloom of the coccolithophore *Emiliania huxleyi*, *Mar. Ecol. Prog. Ser.*, *126*, 247–265, doi:10.3354/meps126247.

Winter, A., and W. G. Siesser (1994), *Coccolithophores*, 242 pp., Cambridge Univ. Press, Cambridge, U. K.

Xu, Y., T. M. Wahlund, L. Feng, Y. Shaked, and F. M. M. Morel (2006), A novel alkaline phosphatase in the coccolithophore *Emiliania huxleyi* (Prymnesiophyceae) and its regulation by phosphorus, *J. Phycol.*, *42*, 835–844, doi:10.1111/j.1529-8817.2006.00243.x.

Young, J. R. (1994), Functions of coccoliths, in *Coccolithophores*, edited by A. Winter and W. G. Siesser, pp. 63–82, Cambridge Univ. Press, Cambridge, U. K.

Zar, J. H. (1974), *Biostatistical Analysis*, 620 pp., Prentice-Hall, Englewood Cliffs, N. J.

Zhang, H., L. Hu, and M.-X. He (2009), Scattering by pure seawater: Effect of salinity, *Opt. Express*, *17*, 5698–5710, doi:10.1364/OE.17.005698.

Zhang, X., M. Lewis, M. Lee, B. Johnson, and G. Korotaev (2002), The volume scattering function of natural bubble populations, *Limnol. Oceanogr.*, *47*, 1273–1282, doi:10.4319/lo.2002.47.5.1273.

D. Alley, W. M. Balch, E. S. Booth, B. C. Bowler, and D. T. Drapeau, Bigelow Laboratory for Ocean Sciences, PO Box 475, 180 McKown Point Rd., West Boothbay Harbor, ME 04575, USA. (bbalch@bigelow.org)

E. Lyczskowski, School of Marine Sciences, University of Maine, Orono, ME 04469, USA.